JOURNAL OF THERMOPHYSICS AND HEAT TRANSFER
Vol. 23, No. 1, January–March 2009

Estimation of Temperature-Dependent Thermophysical Properties of Noncharring Ablators

H. Molavi*
Tarbiat Modares University, 14115-143 Tehran, Iran
A. Hakkaki-Fard†
McGill University, Montreal, Quebec H3A 2K6, Canada
I. Pourshaban‡ and M. Mahbubi Fard§
University of Tehran, 14395-515 Tehran, Iran
and
R. K. Rahmani¶
University of Toledo, Toledo, Ohio 43606

DOI: 10.2514/1.38432

The Levenberg–Marquardt method is used for simultaneously estimating the temperature-dependent thermal conductivity and specific heat of noncharring ablators with moving boundary over a wide temperature range up to 5000 K. It is assumed that no prior information is available on the functional forms of the unknown thermal conductivity and specific heat in the present study. A special feature about the proposed method is that the net surface heat flux and ablative mass flux are unknown a priori and must be determined at each time step. The measured temperatures are simulated numerically by the Charring Material Ablation code that accounts for unsteady ablation. Particular emphasis is placed on the sensitivity analysis, in which the role of sensor location and number of sensors in the estimation of thermal properties can be best appreciated. Considering the nonlinear nature of the proposed inverse problem, it is shown via simulated experiment that unknown parameters can be achieved with reasonable accuracy using this method despite the correlation of the involving parameters and the existing noises in the measurement data.

Nomenclature

a	=	blowing constant
B'	=	dimensionless mass blowing rate
c_p	=	specific heat, J/kg · K
D	=	determinant of the scaled-sensitivity coefficient matrix and its transpose
$\mathrm{d}t$	=	time step, s
h_c	=	enthalpy of solid exposed to ablation, J/kg
h_r	=	recovery enthalpy, J/kg
h_w	=	enthalpy at wall, J/kg
I	=	identity matrix
k	=	thermal conductivity, W/m · K
M	=	number of total time steps
$\dot{m}$	=	ablative mass flux, kg/m^2 · s
N	=	number of sensors
N_P	=	number of unknown parameters
n	=	number of unknown parameters
$\mathbf{P}$	=	vector of unknown parameter
P	=	boundary-layer pressure, atm
$\hat{P}$	=	elements of the covariance matrix in Eq. (20)
q_{cw}	=	cold-wall heat flux, W/m^2
q_{net}	=	net surface heat flux, W/m^2
r	=	element of the correlation matrix in Eq. (20)
S	=	objective functional
s	=	surface recession, m
T	=	temperature, K
T_{ref}	=	reference temperature, K
T_w	=	wall temperature, K
t	=	time, s
t_n	=	duration of the simulated experiment, s
v	=	recession rate, m/s
$\underline{X}$	=	sensitivity matrix
$\bar{X}$	=	scaled-sensitivity matrix
x	=	moving coordinate, m
Y	=	temperature measured by sensors, K
y	=	stationary coordinate, m
ε	=	surface emissivity; or very small value used in Eq. (10)
λ	=	damping parameter used in Eq. (6)
ρ	=	density, kg/m^3
σ	=	Stefan–Boltzmann constant, W/m^2 · K^4; or standard deviation of the errors in the measured temperatures

Superscripts

i	=	number of iteration
T	=	transpose of a matrix

Received 7 May 2008; revision received 21 August 2008; accepted for publication 24 August 2008.

*Graduate Student; currently Faculty of Engineering, Department of Mechanical Engineering; hn.molavi@gmail.com.
†Ph.D. Candidate, Department of Mechanical Engineering; ali.hakkaki-fard@mail.mcgill.ca.
‡Graduate Student, Department of Chemical Engineering.
§Graduate Student, Department of Mechanical Engineering.
¶Affiliate Research Scholar, Mechanical, Industrial, Manufacturing Engineering Department; rkhrahmani@yahoo.com.

I. Introduction

ABLATIVE materials are usually categorized as noncharring and charring ablators. Noncharring ablators are nondecomposing ablators that only chemically erode, oxidize, or change phase at the exposed surface. These materials can generally withstand higher shear stresses than charring ablators. Charring or decomposing ablators are typically resin/fiber composites that are less dense than noncharring ablators and are structurally weaker. These materials undergo both surface erosion and in-depth decomposition. When in-depth temperatures are sufficiently high, the resin (and sometimes the

fiber material) pyrolyzes, creating porous charred solid and gas that is free to move within the material and out to the surface, depending on in-depth pressure gradients.

Thermophysical properties of ablative materials are extremely important for forecasting their performance in working conditions. These properties' values have a significant influence on the temperature distribution and heat flow rate. The limitation of the experimental methods in determining thermal properties of ablative materials, due to their harsh working conditions, leads to the use of inverse parameter estimation (IPE) techniques. Parameter estimation methods are noninvasive techniques that allow for the simultaneous estimation of the thermal properties of individual materials as well as complex structures for any kind of appropriate experiments, provided that these are feasible and that a mathematical model can be formulated. These methods are based on the minimization of an objective function containing both calculated and measured temperatures. The parameters (i.e., thermal properties) that minimize the aforementioned function are the solution of the inverse problem.

Any IPE algorithm, regardless of its theoretical approach, requires the usage of a well-established solution routine for direct problem calculations. This solution routine may be called upon numerous times by the main IPE computational routine. Therefore, the use of highly efficient, as well as accurate, direct calculation schemes is essential in any IPE technique. A large number of investigations have been performed concerning the behavior and modeling of heat transfer in ablative materials. The computer codes such as the Heat Balance Integral [1,2], the Charring Material Ablation (CMA) [3], the Fully Implicit Ablation and Thermal Response [4], and the Control Volume Finite Element Spatial Discretization Method [5] determine the thermal response of an ablative heat shield by solving equations in one-dimensional space.

Estimation of thermal properties of solids has been the subject of extensive investigations because of their numerous and varied applications. Beck [6] estimated the thermal conductivity simultaneously with the volumetric heat capacity of nickel from one-dimensional transient temperature measurements. Beck and Arnold [7] developed a procedure for determining the thermal properties from transient temperature and heat flux measurements. Huang and Özisik [8] obtained precise estimations for 1-D solids in the case of linear and sinusoidal dependencies of both properties using approximate direct integration method. Beck and Osman [9] used a method to sequentially estimate thermal properties by mathematically connecting a series of discrete experiments with various temperature ranges. Dowding et al. [10] determined the temperature-dependent thermal properties of carbon composites from transient temperature and heat flux measurements. Huang and Yan [11] also obtained estimations of the same dependencies using the conjugate gradient method of minimization and the adjoint equation. Sawaf et al. [12] estimated these properties in a 2-D orthotropic solid using Levenberg–Marquardt's iterative procedure. Dantas and Orlande [13] used a function estimation technique, which assumes that the form of the function is known, to estimate these properties by applying the conjugate gradient method. Dowding et al. [14] analyzed a series of discrete independent experiments in a sequential manner to estimate temperature-dependent thermal properties of carbon–carbon composite. Garcia [15] used genetic algorithms to estimate the temperature-dependent thermal properties of carbon/epoxy anisotropic composites. Alhama et al. [16] used the network simulation method as the numerical tool and three points of measurement in the solid for simultaneous estimation of thermal conductivity and specific heat.

The present approach is unlike traditional methods appearing in the literature, because it does not require prescribed time-dependent surface heat flux. This function depends on the thermophysical properties and wall temperature and recovers as part of the formulation. In addition, the temperature ranges in the cited literature are below the temperatures at which surface thermochemical processes are significant enough to cause feasible surface recession. As the temperature rises, noncharring ablators can experience one or several transformations, typically oxidation and sublimation, depending on the incident heat flux variation and the material characteristics. Thus, a moving boundary will appear in the ablation process. There are few publications available in literature on the inverse problems in ablative composites with moving boundary. One notable work in this field includes [17], which is a function estimation solution of surface heat flux in a charring ablator. It is interesting to note that the transient function estimation for simultaneously measuring temperature-dependent thermal conductivity and specific heat for ablative materials without preassumed surface heat flux, which has a moving boundary, has never been examined in the open literature. To address this problem, the authors have developed a numerical analysis capability to study the transient heating and chemical evolution of surfaces under ablative flow conditions, which involves a moving boundary that is not known a priori. In addition, no prior information on the functional forms of the unknown quantities is necessary in inverse calculations.

The accuracy of the estimated properties is directly related to the sensitivity of the temperature distribution with respect to the thermal properties and can be increased if the experiments are carefully designed [7]. Small magnitudes of the sensitivity coefficients and near-linear dependence among the coefficients are limiting factors to the stability, and thus to the convergence, of gradient-based estimation procedures. Several different approaches have been used to address this correlation-based nonconvergence problem. One approach is to modify the experimental design. Loh and Beck [18] used several thermocouples at various locations within the sample to bypass the correlation problem. Another approach used to address the correlation problem is to modify the minimization method. Copenhaver et al. [19] used a constrained parameter estimation procedure based on a penalty function method, with limited success, to simultaneously estimate three nearly correlated thermal properties of a honeycomb sandwich structure. Another approach is to use a nongradient method. Garcia [15] used genetic algorithms to circumvent difficulties of nonconvergence in cases when the parameters are correlated or nearly so.

In the present work, sensitivity analysis is investigated to improve experimental conditions (i.e., number of sensors and sensor placement) in the determination of thermal properties. The measured temperatures are simulated using the CMA code that accounts for unsteady ablation. Uncertainty in temperature measurements is modeled as stationary zero-mean white noise. These data are processed using the Levenberg–Marquardt method for simultaneously determining the temperature-dependent thermal conductivity and specific heat in noncharring ablators without the need for any prior information on the kind of dependence of these properties.

II. Direct Problem

This section presents a summary of the equations for noncharring ablators and a brief outline of the numerical procedures.

A. Internal Energy Balance Equation

For the one-dimensional heat transfer simulation of the noncharring ablator, the internal energy balance can be written as

$$\rho c_p \frac{\partial T}{\partial t} = \frac{\partial}{\partial x}\left(k\frac{\partial T}{\partial x}\right) + \rho c_p v \frac{\partial T}{\partial x} \tag{1}$$

where the material properties c_p and k are taken as known functions of T, and material density ρ is generally constant.

B. Surface Energy Balance Equation

The boundary conditions at the ablating surface are determined from the surface energy balance. The net heat flux transferred to the wall surface is given by

$$q_{\text{net}} = q_{\text{cw}}\left(\frac{aB'}{\exp(aB')-1}\right)\left(1-\frac{h_w}{h_r}\right) - \sigma\varepsilon\left(T_w^4 - T_{\text{ref}}^4\right) - \dot{m}(h_w - h_c) \tag{2}$$

Fig. 1 Initial-to-final grid comparison.

The first term on the right-hand side of Eq. (2) represents the sensible convective heat flux, where B' and h_w are the functions of surface temperature and pressure. To generate tables of B' and h_w for ablative materials, the Aerotherm Chemical Equilibrium (ACE) [20] or Multicomponent Ablation Thermochemistry [21] codes can be used. The second and third terms on the right-hand side of Eq. (2) are the radiative heat fluxes reradiated by the wall and ablative contribution, respectively.

C. Numerical Approach

The computational grid, with the exception of the last ablating node, consists of equally spaced grid nodes along the x axis. The last ablating node has a variable thickness that changes due to surface recession. The grid attaches to the receding surface, and each node translates with the same velocity as the surface. The overall number of nodes in the domain is reduced as mass is removed at the ablating surface. The last node is eliminated when its thickness falls below a predefined threshold. Figure 1 conceptually shows an initial-to-final grid comparison for a one-dimensional uniformly spaced grid.

The internal energy balance equation is discretized using the second-order-in-space and first-order-in-time finite difference method. These equations are implicit in temperature. Because the internal energy balance equation is nonlinear in both surface recession rate and temperature, a linearization method is used to find a solution. This is done by lagging the thermophysical properties and surface recession rate one time step for the interior node equations. Then Eq. (1) can be written in finite difference form as

$$\frac{\rho C p_i^n (T_i^{n+1} - T_i^n)}{\Delta t} = \frac{1}{\Delta x_i}\left(\frac{T_{i+1}^{n+1} - T_i^{n+1}}{\frac{\Delta x_{i+1}}{2}\frac{1}{k_{i+1}^n} + \frac{\Delta x_i}{2}\frac{1}{k_i^n}} - \frac{T_i^{n+1} - T_{i-1}^{n+1}}{\frac{\Delta x_i}{2}\frac{1}{k_i^n} + \frac{\Delta x_{i-1}}{2}\frac{1}{k_{i-1}^n}}\right) + \rho v C p_i^n \left(\frac{T_{i+1}^{n+1} - T_{i-1}^{n+1}}{2\Delta x_i}\right) \tag{3}$$

Rearrangement and applying boundary conditions allow the preceding discretization equations to be as follows:

$$a_i T_{i-1} + b_i T_i + c_i T_{i+1} = d_i \quad \text{for } i = 1, 2, \ldots, L \tag{4}$$

where L denotes the number of nodes. Using a tridiagonal matrix algorithm, a lower triangular form of the preceding matrix may be obtained as follows:

$$b_i = b_i - \frac{a_{i+1}}{b_{i+1}} c_i, \qquad d_i = d_i - \frac{d_{i+1}}{b_{i+1}} c_i \tag{5}$$

One of the key purposes of the in-depth response solution is to provide a function of surface temperature for the net surface heat flux, which plays the central role in linking the in-depth solution to the surface energy balance equation (2). Then Eq. (2) will become nonlinear with one unknown, T_w, and an iterative solution procedure is necessary to solve for the surface temperature (see [3] for more details).

III. Inverse Problem

In the inverse problem considered in this study, the thermal properties $k(T)$ and $c_p(T)$ are regarded as being unknown and to be estimated from measured temperatures of sensors. These unknown ablation parameters are gathered in a single unknown vector $\mathbf{P} = [k(T), c_P(T)]$.

The solution of the present inverse problem is to be obtained in such a way that the following function is minimized:

$$S(\mathbf{P}) = \sum_{i=1}^{N}\sum_{j=1}^{M}(Y_{i,j} - T_{i,j}(\mathbf{P}))^2 \tag{6}$$

where $Y_{i,j}$ are the measured temperatures, $T_{i,j}$ are the estimated temperatures at the measurement locations obtained by the developed CMA code, M is the number of total time steps, and N is the number of used sensors.

Because of the temperature dependence of thermal properties and the moving nature of an ablative boundary, the current inverse problem is a nonlinear parameter estimation problem. Thus, an iterative inverse method is required. One of the prevalent iterative methods to minimize the objective function S is the Levenberg–Marquardt Method (LMM) [22], which is described in the next section.

IV. Computational Procedure for Inverse Method

The inverse solution algorithm based on LMM is an iterative method, and the computational procedure for the estimation of the unknown parameters at iteration i can be summarized as follows (more details can be found in [22]):

1) Solve the direct problem with available estimated $k(T)$ and $c_p(T)$ to obtain temperature field in the noncharring ablator $T(\mathbf{P}^{(i)})$.

2) Compute S from Eq. (6).

3) Compute the sensitivity matrix X defined by the following equation:

$$X = \begin{bmatrix} \frac{\partial T_1}{\partial P_1} & \frac{\partial T_1}{\partial P_2} & \cdots & \frac{\partial T_1}{\partial P_n} \\ \frac{\partial T_2}{\partial P_1} & \frac{\partial T_2}{\partial P_2} & \cdots & \frac{\partial T_2}{\partial P_n} \\ \vdots & \vdots & \cdots & \vdots \\ \frac{\partial T_N}{\partial P_1} & \frac{\partial T_N}{\partial P_2} & \cdots & \frac{\partial T_N}{\partial P_n} \end{bmatrix} \tag{7}$$

where P_1 to P_n denote the components of the unknown vector $\mathbf{P}$.

4) Solve the following linear system of equation for finding $\Delta\mathbf{P}^{(i)}$:

$$[\lambda^{(i)} I + X^{T(i)} X^{(i)}]\Delta\mathbf{P}^{(i)} = X^{T(i)}(\mathbf{T}^{(i)} - \mathbf{Y}^{(i)}) \tag{8}$$

where superscript T denotes the transpose sign, and vectors $\mathbf{T}$ and $\mathbf{Y}$ are defined as

$$\mathbf{T}^{(i)} = [T_{1,1}, T_{1,2}, \ldots, T_{1,M}, T_{2,1}, T_{2,2}, \ldots, T_{2,M}, \ldots, T_{N,M}]^{(i)} \tag{9}$$

$$\mathbf{Y}^{(i)} = [Y_{1,1}, Y_{1,2}, \ldots, Y_{1,M}, Y_{2,1}, Y_{2,2}, \ldots, Y_{2,M}, \ldots, Y_{N,M}]^{(i)} \tag{10}$$

in this study, the initial value for $\lambda^{(i)}$ is set to 0.01.

5) The updating rule for the LMM algorithm is then applied to determine the unknown vector:

$$\mathbf{P}^{(i+1)} = \mathbf{P}^{(i)} + \Delta\mathbf{P}^{(i)} \tag{11}$$

6) Solve the direct problem with this new estimated $\mathbf{P}^{(i+1)}$ to obtain $T(\mathbf{P}^{(i+1)})$, then compute S, as defined by Eq. (6).

7) If $S(\mathbf{P}^{(i+1)}) \geq S(\mathbf{P}^{(i)})$, replace $\lambda^{(i)}$ with $10 \cdot \lambda^{(i)}$ and return to step 4.

8) If $S(\mathbf{P}^{(i+1)}) < S(\mathbf{P}^{(i)})$, accept the new estimate $\mathbf{P}^{(i+1)}$ and replace $\lambda^{(i)}$ with $0.1 \cdot \lambda^{(i)}$.

9) Check the stopping criteria given by Eq. (12):

$$S(\mathbf{P}^{(n)}) < \varepsilon \tag{12}$$

Stop the iteration procedure if it is satisfied; otherwise, replace i with $i + 1$ and return to step 3.

If the measured temperatures contained no random errors (noise), the ε in Eq. (12) can be chosen as an arbitrary small value. When the measured temperatures contain noise, as in a real experiment, one

cannot expect the function Eq. (6) to become equal to zero at the final iteration step. Therefore, following the suggestions made by Oliveira and Orlande [23] and Colaco and Orlande [24], the following expression for ε was used in this study

$$\varepsilon = N \cdot M \cdot \sigma^2 \tag{13}$$

where σ is the standard deviation of the errors in the temperature.

V. Result and Discussions

To examine the proposed procedure for the inverse estimations of the temperature-dependent thermal properties in the temperature range from 300 to 5000 K, we use a test case taken from [1]. The considered domain in this example extended from 0 to 5 cm. The ablative material is carbon–carbon with properties as given in Table 1. Thermal conductivities and specific heats are considered as constants for different temperatures, and linear regressions are generated to express these properties as functions of temperature. The aeroheating inputs for this test case are given in terms of cold-wall heat flux q_{cw}, recovery enthalpy h_r, and boundary-layer pressure P (Fig. 2).

Ablative mass flux and wall enthalpy may be a complex function of surface temperature and pressure. In this work, a set of pressure and temperature-dependent correlations to ACE [20] computer calculations (developed by Potts [1]) are used to estimate mass flux and wall enthalpy. Figure 3 shows the variation of dimensionless mass blowing rate and wall enthalpy as a function of temperature for a range of pressures.

In the inverse calculations considered here, the temperature measurements $Y(t)$ are known from numerical simulations obtained by the developed CMA code. These data are taken every 0.1 s over the time range 0–30 s. It is assumed that the tungsten–rhenium (C-type) thermocouples are used in this simulated experiment, which can sustain high temperature up to 2500 K. It should be noted that due to high temperature in the areas near the ablating surface and its deterioration during the experiment, sensors cannot withstand such a harsh condition and burn out. In this situation, it is assumed that the burned-out sensor returns zero values; hence, it does not affect the mathematical formulation given previously.

In the first part of this section, verification of the developed CMA code is considered. In the second part, the sensitivity analysis is investigated to provide insight into the estimation problem. In the last part, the estimation results obtained by applying the proposed method are given and discussed.

A. Direct Code Verification

To verify the numerical solutions obtained, a postprocessing procedure based on the Richardson extrapolation as described by Roache [25] has been used to confirm the spatial order of accuracy of the solution procedure. To accomplish this, the studied domain was discretized using four different uniform grids. Because the temporal discretization is expected to be first order and the spatial discretization is expected to be second order, it will be assumed that the discretization error (DE) can be expressed by

$$\mathrm{DE} = \Delta x^2 \left(a + \frac{b \Delta t}{\Delta x^2} \right) + (\text{higher-order terms}) \tag{14}$$

As a result, ignoring the higher-order terms, if the spatial and temporal grids are simultaneously refined while keeping $\Delta t / \Delta x^2$ constant, then the spatial and temporal orders of accuracy can be confirmed whether the grid convergence is second order or not. The grid parameters for the four grids with $\Delta t / \Delta x^2 = 1.25$ s/cm^2 can be seen in Table 2. If it is assumed that the discretization method is second order spatially and that the two grids used to generate the solutions for the extrapolation procedure have the relationship

$$\frac{\Delta x_2}{\Delta x_1} = 2 \tag{15}$$

Table 1 Carbon–carbon thermal properties

Temperature, K	Thermal conductivity, W/m · K	Specific heat, J/kg · K	Density, kg/m^3
300	123.6	720	1900
400	116.5	990	1900
600	102.8	1410	1900
800	90.6	1650	1900
1000	80.3	1790	1900
1200	71.6	1890	1900
1400	64.9	1950	1900
1600	59.8	2040	1900
1800	57	2070	1900
2000	55.1	2100	1900
2200	53.8	2130	1900
2400	53.1	2160	1900
5000	50	2230	1900

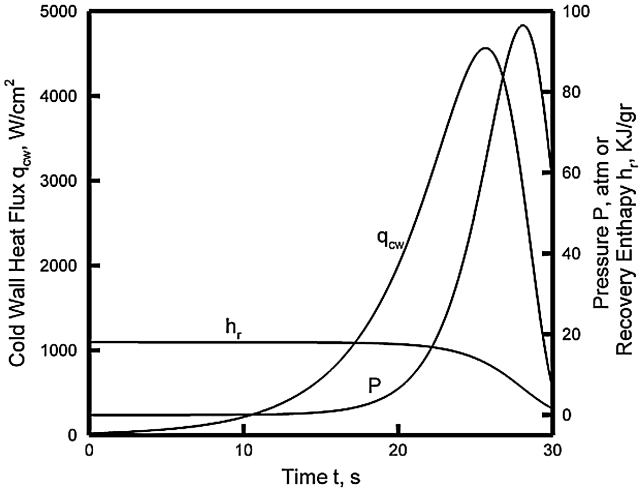

Fig. 2 Aeroheating environment.

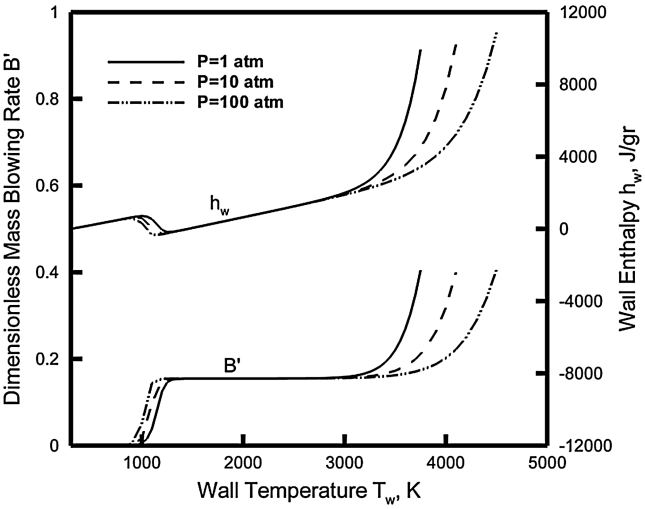

Fig. 3 Dimensionless mass blowing rate and wall enthalpy as a function of temperature and pressures.

Table 2 Grid parameters for spatial refinement

Grid	No. nodes	Δx, cm	Δt, s
4	126	0.04	0.2
3	251	0.02	0.05
2	501	0.01	0.0125
1	1001	0.005	0.003125

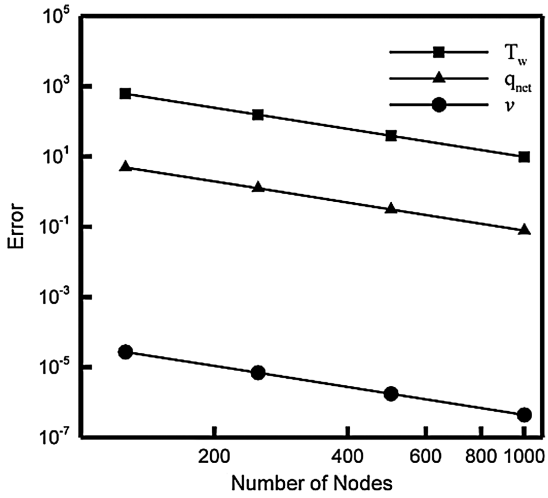

Fig. 4 Richardson extrapolation grid convergence results.

then the exact solution is fourth-order-accurate and can be approximated by

$$f_{\text{exact}} \cong f_1 + \frac{f_1 - f_2}{3} \tag{16}$$

where f_1 and f_2 are the original solutions for the grid spacing Δx_1 and Δx_2, respectively.

This procedure is performed on the surface temperature, net surface heat flux, and surface recession. The errors in surface temperature, net surface heat flux, and recession rate are then computed at an elapsed time of 30 s for each of the four grids. Figure 4 shows the relationship between the grid spacing and the error for some selected characteristic quantities. Second-order grid convergence for three error metrics can be seen in this figure.

Although it is not a part of the formal verification process, it is sometimes beneficial to perform code-to-code comparisons throughout the development process. For this purpose, the ablation verification problem solves on the grid spacing Δx_3 in Table 2. Then our results are compared with the corresponding results presented in [1], which are based on the finite difference method. Figure 5 shows good agreement between present results and finite difference (FD) calculations.

B. Sensitivity Analysis

Sensitivity coefficient is the first derivative of temperature with respect to the estimated property. Its analysis allows improvement of an experimental design to be used in determination of properties by selecting experimental conditions in the mathematical model. Experimental parameters such as sensor location and number of sensors are important factors to be considered in the design.

In general, the scaled-sensitivity coefficients are desired to be large and uncorrelated (linearly independent) for different parameters. A sense of the magnitude of the sensitivity coefficients is gained through normalizing the sensitivity coefficients. Normalization is performed by multiplying by the parameters, resulting in units of temperature for all the scaled-sensitivity coefficients. The scaled-sensitivity coefficient for parameter P_1 is

$$\bar{X}_{P_1} = P_1 \frac{\partial T}{\partial P_1} \tag{17}$$

When two or more parameters are unknown, the use of the magnitude of the individual scaled-sensitivity coefficients as a reference becomes messy, and therefore the design activity needs to be posed in terms of an optimality criterion to maximize. Among the different design criteria, the maximization of the determinant of Fisher information matrix $X^T X$ (D-optimality criterion) is the most commonly used and is often recommended [6,19,26–30]. The constraint of a fixed large number of equally spaced measurements can be incorporated in the determinant of the Fisher information matrix by defining a normalize sensitivity matrix by

$$D = |[d_{ij}]| \tag{18}$$

where

$$d_{ij} = \frac{1}{Nt_n} \sum_{r=1}^{N} \int_0^{t_n} \left(P_i \frac{\partial T}{\partial P_i} \right) \left(P_j \frac{\partial T}{\partial P_j} \right) \mathrm{d}t \tag{19}$$

The scaled-sensitivity coefficients are computed using a finite difference approximation on the temperature output of the CMA code. The initial guess of 50 $\mathrm{W/m \cdot K}$ for thermal conductivities and 2000 $\mathrm{J/kg \cdot K}$ for specific heats is used. The determinant D is calculated from Eq. (18) for various sensor locations and is shown in Fig. 6.

The results indicate that the sensors that are closer to the original surface have higher determinant values; however, they burn out faster. Figure 7 illustrates the interior temperature distribution of the material at elapsed times of 15, 20, 25, and 30 s. Hence, the sensor location in the range from 0.3 to 1 cm is a good choice.

The correlation matrix for the sensor location is determined based on the procedure described by Beck and Arnold [7]. The elements of the correlation matrix are given by

$$r_{ij} = \frac{\hat{P}_{ij}}{\sqrt{\hat{P}_{ii}\hat{P}_{jj}}} \qquad i = 1, \ldots, N_P, \qquad j = 1, \ldots, N_P \tag{20}$$

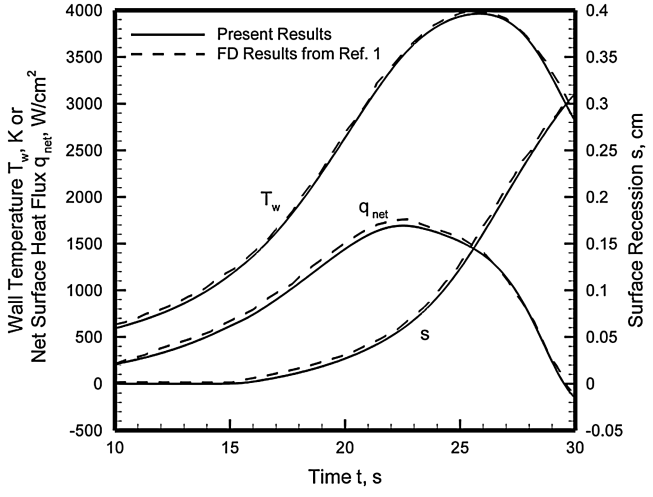

Fig. 5 Comparison of FD and CMA solutions.

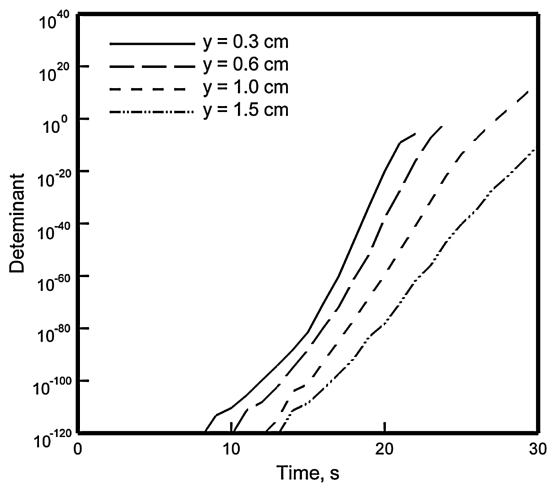

Fig. 6 Effect of various sensor locations on the determinant.

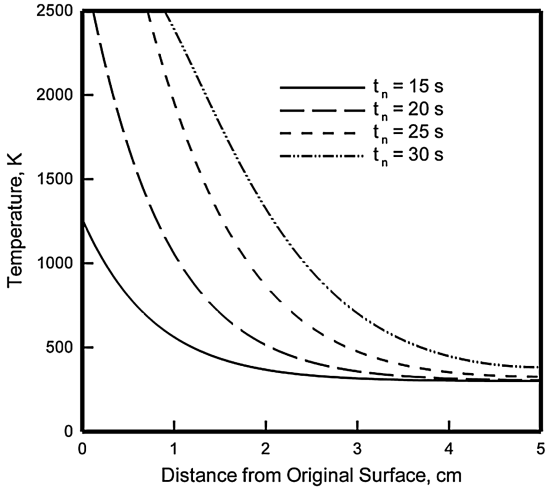

Fig. 7 Temperature profiles inside the sample for various times.

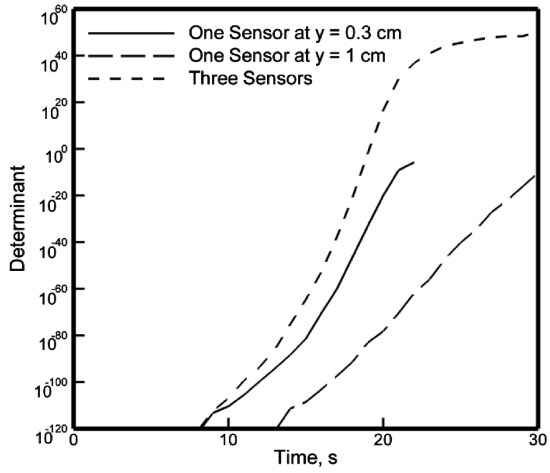

Fig. 8 Effect of the using three sensors on the determinant value.

where $\hat{P}_{ij}$ represents the elements of the covariance matrix of the estimated parameters given by $\sigma^2(X^TX)^{-1}$. When one sensor is applied, near-linear dependency among a numbers of unknown parameters can be observed. The use of several sensors within the sample bypasses the correlation problem. This is why three sensors were used in this study, for which the centers were located at 0.3, 0.6, and 0.9 cm. Moreover, this choice considerably improves the determinant value, as indicated in Fig. 8. Figure 9 illustrates temperature predictions by the developed CMA code for these sensors. It can be observed that the first, second, and third sensors are burned out after 21.5, 24, and 27.5 s, respectively.

Because of the large number of unknown parameters, rather than show the complete correlation matrix (26×26) for this problem, it would more appropriate to just display near-linear dependence among the parameters. Because correlation is not encountered among the unknown parameters of specific heat and thermal conductivity, the correlation matrix for specific heat and thermal conductivity parameters are shown separately in Tables 3 and 4, respectively.

As it is seen, on one hand, the number of the correlated parameters for specific heat is larger than those for thermal conductivity. On the other hand, there is linear dependency just between three thermal conductivity parameters. So the convergence and the solution of the parameter estimation will not be easily obtained. Moreover, there is a possibility that the estimated values of correlated parameters differ from their real values, but they yield the same result.

C. Parameter Estimation Results

The number of sensors used for this problem by which reasonable results could be obtained was three sensors, as previously noted; therefore, the total number of temperature readings that were taken in this simulation according to the sensors limitations was 903 samples.

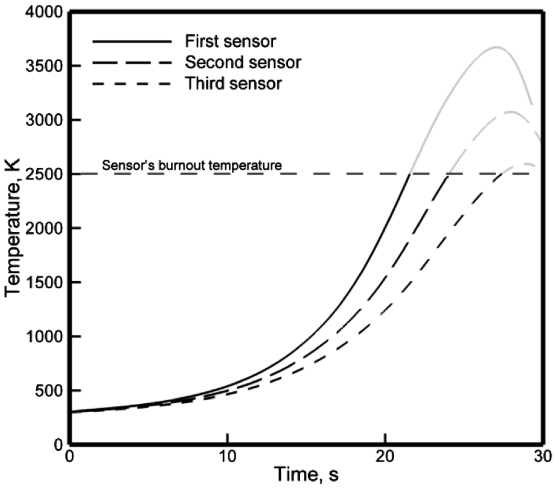

Fig. 9 Temperature used for parameter estimation.

Three simulated sets of data are used in this study: 1) errorless data by which the inverse algorithm is tested, 2) data containing errors having a Gaussian distribution with standard deviation equal to 0.2% of the maximum temperature (corresponding roughly to a 5 K error), and 3) data containing errors having a Gaussian distribution with standard deviation equal to 0.5% of the maximum temperature (corresponding roughly to a 12.5 K error).

As previously mentioned, the net surface heat flux and recession rate are not known a priori and must be calculated at each time step. The initial guess of 50 $W/m \cdot K$ for thermal conductivities and 2000 $J/kg \cdot K$ for specific heats yields different values for these parameters, as seen in Fig. 10.

Table 3 Correlation matrix for specific heat

Parameters	c_{p300}	c_{p400}	c_{p600}	c_{p800}	c_{p1000}	c_{p1200}	c_{p1400}	c_{p1600}	c_{p1800}	c_{p2000}	c_{p2200}	c_{p2400}	c_{p5000}
c_{p300}	1	——	——	——	——	——	——	——	——	——	——	——	sym.
c_{p400}	0.82	1	——	——	——	——	——	——	——	——	——	——	——
c_{p600}	0.65	0.93	1	——	——	——	——	——	——	——	——	——	——
c_{p800}	0.56	0.81	0.94	1	——	——	——	——	——	——	——	——	——
c_{p1000}	0.51	0.75	0.87	0.97	1	——	——	——	——	——	——	——	——
c_{p1200}	0.46	0.68	0.80	0.90	0.97	1	——	——	——	——	——	——	——
c_{p1400}	0.43	0.63	0.74	0.84	0.92	0.98	1	——	——	——	——	——	——
c_{p1600}	0.39	0.58	0.68	0.77	0.86	0.93	0.98	1	——	——	——	——	——
c_{p1800}	0.36	0.54	0.64	0.73	0.81	0.88	0.94	0.98	1	——	——	——	——
c_{p2000}	0.30	0.44	0.52	0.60	0.67	0.73	0.79	0.88	0.85	1	——	——	——
c_{p2200}	−0.17	−0.26	−0.30	−0.35	−0.39	−0.43	−0.47	−0.55	−0.47	−0.85	1	——	——
c_{p2400}	0.23	0.35	0.42	0.48	0.53	0.58	0.64	0.73	0.67	0.96	−0.96	1	——
c_{p5000}	0.19	0.29	0.35	0.40	0.44	0.49	0.53	0.62	0.54	0.88	−0.99	0.97	1

Table 4 Correlation matrix for thermal conductivity

Parameters	k_{300}	k_{400}	k_{600}	k_{800}	k_{1000}	k_{1200}	k_{1400}	k_{1600}	k_{1800}	k_{2000}	k_{2200}	k_{2400}	k_{5000}
k_{300}	1	——	——	——	——	——	——	——	——	——	——	——	sym.
k_{400}	0.29	1	——	——	——	——	——	——	——	——	——	——	——
k_{600}	0.10	0.65	1	——	——	——	——	——	——	——	——	——	——
k_{800}	0.19	0.27	0.57	1	——	——	——	——	——	——	——	——	——
k_{1000}	0.07	0.20	0.22	0.57	1	——	——	——	——	——	——	——	——
k_{1200}	0.04	0.08	0.10	0.17	0.59	1	——	——	——	——	——	——	——
k_{1400}	0.01	0.02	0.01	0.04	0.18	0.60	1	——	——	——	——	——	——
k_{1600}	−0.05	−0.13	−0.16	−0.18	−0.12	0.07	0.54	1	——	——	——	——	——
k_{1800}	0.02	0.04	0.041	0.04	0.07	0.13	0.34	0.42	1	——	——	——	——
k_{2000}	−0.11	−0.26	−0.31	−0.34	−0.38	−0.38	−0.43	−0.06	−0.66	1	——	——	——
k_{2200}	0.08	0.19	0.22	0.24	0.28	0.28	0.38	0.09	0.80	−0.94	1	——	——
k_{2400}	−0.09	−0.22	−0.26	−0.29	−0.33	−0.34	−0.42	−0.11	−0.79	0.96	−0.99	1	——
k_{5000}	−0.07	−0.17	−0.21	−0.22	−0.26	−0.26	−0.35	−0.06	−0.78	0.94	−0.99	0.97	1

First, the estimated results for noise-free data are presented. Table 5 shows the estimated parameters obtained from errorless data. Despite the existence of correlations among a numbers of properties, applying the proposed method will yield very precise results. Furthermore, the net surface heat flux and recession rate matched well with the exact values. These results verify the validity of the proposed parameter estimation procedure. At the next stage, thermal properties are estimated considering the noisy data. The results are presented for different levels of measurement errors in Tables 6 and 7, respectively. Two issues can be concluded from these tables: First, the errors in the estimated parameters increased as the standard deviation of the temperature measurement error increased. Second, the thermal conductivities are estimated better than specific heats, as prospected.

Figure 11 shows differences between the estimated values of net heat flux and recession rate at the end of estimation procedure and the exact values. These differences show a source of error in the parameter estimation problem.

Figure 12 compares the reduction of the objective function with respect to the number of iterations for three case studies. As it is seen, the number of iterations is about three to six times, which shows that the convergence speed is fast. To show $k(T)$ and $cp(T)$ more explicitly as functions of temperature, the exact and estimated thermal conductivities and specific heats for different sets of data are presented in Figs. 13 and 14, respectively. As expected, the increases in the measurement errors cause decreases in the accuracy of the inverse solution.

VI. Conclusions

The Levenberg–Marquardt method was successfully applied for simultaneously predicting temperature-dependent thermal

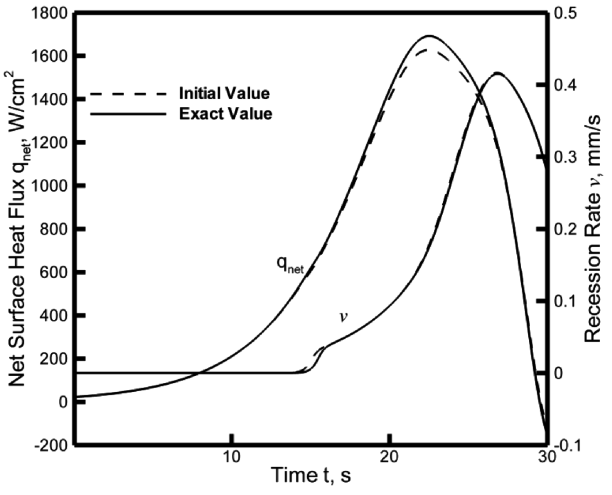

Fig. 10 Comparison between the initial value of net surface heat flux and recession rate and exact values.

Table 5 Estimated parameters for errorless data

Temperature, K	Thermal conductivity, W/m · K	Specific heat, J/kg · K
300	123.60	720.00
400	116.51	989.99
600	102.79	1410.00
800	90.59	1649.99
1000	80.29	1790.00
1200	71.60	1889.99
1400	64.90	1950.00
1600	59.79	2039.99
1800	56.99	2070.00
2000	55.10	2100.00
2200	53.80	2129.99
2400	53.09	2159.99
5000	50.00	2229.99

Table 6 Estimated parameters for noisy data ($\sigma = 0.0002\ T_{max}$)

Temperature, K	Thermal conductivity, W/m · K	Percent error	Specific heat, J/kg · K	Percent error
300	118.88	3.82	705.41	2.03
400	116.11	0.34	1018.29	2.86
600	103.09	0.28	1373.47	2.59
800	91.96	1.50	1690.85	2.48
1000	79.13	1.46	1677.74	6.27
1200	71.23	0.51	1996.06	5.61
1400	65.50	0.93	2001.49	2.64
1600	59.55	0.41	1932.34	5.28
1800	57.26	0.45	2157.03	4.20
2000	55.23	0.24	2066.57	1.59
2200	53.99	0.36	2100.32	1.39
2400	52.46	1.20	2127.07	1.52
5000	50.64	1.29	2068.61	7.24

Table 7 Estimated parameters for noisy data ($\sigma = 0.0005\ T_{max}$)

Temperature, K	Thermal conductivity, W/m · K	Percent error	Specific heat, J/kg · K	Percent error
300	115.23	6.77	680.14	5.54
400	115.40	0.94	1062.43	7.32
600	103.65	0.82	1321.86	6.25
800	94.08	3.84	1748.92	6.00
1000	77.33	3.70	1511.81	15.54
1200	70.73	1.21	2156.04	14.08
1400	66.36	2.26	2069.17	6.11
1600	59.24	0.93	1789.46	12.28
1800	57.62	1.08	2266.93	9.51
2000	55.39	0.53	2000.31	4.75
2200	54.33	0.98	2123.46	0.31
2400	51.62	2.78	2044.78	5.33
5000	51.64	3.29	2046.22	8.24

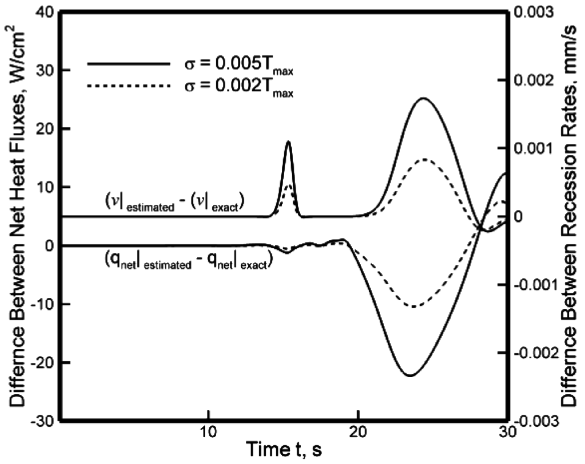

Fig. 11 Difference between estimated net surface heat flux and recession rate at the end of parameter estimation procedure and exact values for different levels of measurements error.

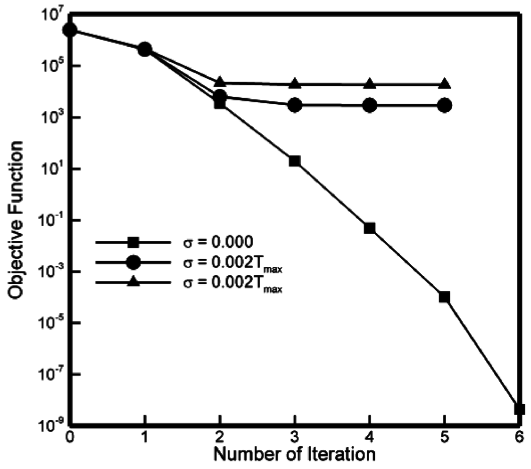

Fig. 12 Reduction histories of the objective function for various cases.

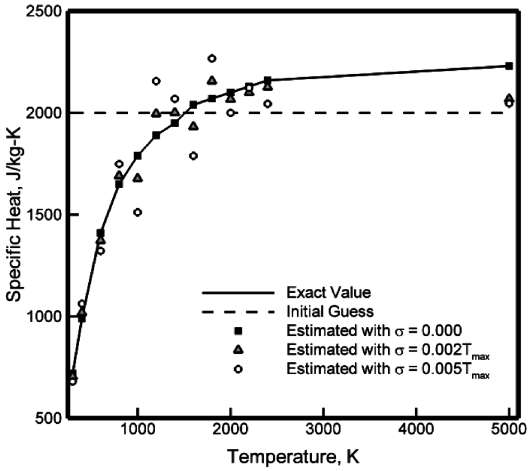

Fig. 13 Exact and estimated values of $c_p(T)$.

conductivity and specific heat of noncharring ablators by using simulated temperature readings. Verification of the method was conducted using carbon–carbon with known thermal properties. The main conclusions can be summarized as follows:

1) The proposed method does not require any assumption on the functional form of the thermal conductivity and specific heat. Moreover, moving boundary is not needed to be known a priori and exact knowledge about the net surface heat flux is not necessary.

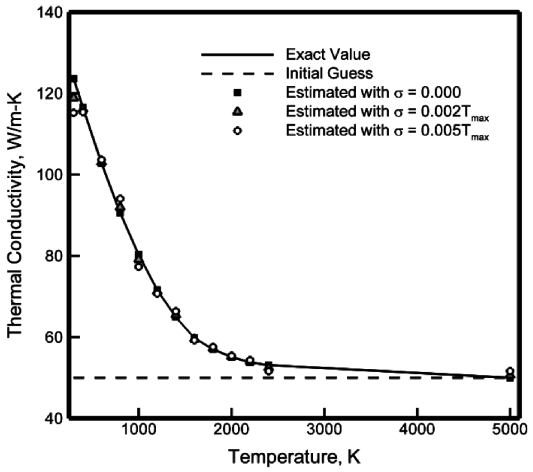

Fig. 14 Exact and estimated values of $k(T)$.

2) The number of iterations is within three to six times, which shows a high speed of convergence.

3) The close agreement between the exact solutions and the estimated results from errorless data shows the potential of the proposed method in finding the accurate values of the temperature-dependent thermal properties in an inverse heat conduction problem. Furthermore, the accuracy of the estimated results from noisy data is reasonable, even when the surface heat flux and the recession rate do not recover their exact values.

4) Despite the limitation of sensors acquiring temperature range, thermophysical properties are estimated over a wide temperature range. This makes the proposed method efficient to predict thermal properties of noncharring ablators at high temperatures.

Acknowledgment

The authors would like to thank Hamid Parhizkar, Ph.D. Student of Amir Kabir University, for reading the initial draft of the manuscript and offering some useful suggestions.

References

[1] Potts, R. L., "Application of Integral Methods to Ablation Charring Erosion, A Review," *Journal of Spacecraft and Rockets*, Vol. 32, No. 2, 1995, pp. 200–209. doi:10.2514/3.26597

[2] Leone, S. A., Potts, R. L., and Laganelli, A. L., "Enhancements to Integral Solutions to Ablation and Charring," *Journal of Spacecraft and Rockets*, Vol. 32, No. 2, 1995, pp. 210–216. doi:10.2514/3.26598

[3] Moyer, C. B., and Rindal, R. A., "An Analysis of the Coupled Chemically Reacting Boundary Layer and Charring Ablator, Part II, Finite Difference Solution for the In-Depth Response of Charring Materials Considering Surface Chemical and Energy Balances," NASA CR-1061, June 1968.

[4] Chen, Y.-K., and Milos, F. S., "Ablation and Thermal Response Program for Spacecraft Heatshield Analysis," *Journal of Spacecraft and Rockets*, Vol. 36, No. 3, 1999, pp. 475–483. doi:10.2514/2.3469

[5] Amar, A. J., Blackwell, B. F., and Edwards, J. R., "One-Dimensional Ablation Using a Full Newton's Method and Finite Control Volume Procedure," *Journal of Thermophysics and Heat Transfer*, Vol. 22, No. 1, 2008, pp. 71–82. doi:10.2514/1.29610

[6] Beck, J. V., "Transient Determination of Thermal Properties," *Nuclear Engineering and Design*, Vol. 3, No. 3, 1966, pp. 373–381. doi:10.1016/0029-5493(66)90128-2

[7] Beck, J. V., and Arnold, K. J., *Parameter Estimation in Engineering and Science*, Wiley, New York, 1977.

[8] Huang, C. H., and Özisik, M. N., "Direct Integration Approach for Simultaneously Estimating Temperature Dependent Thermal Conductivity and Heat Capacity," *Numerical Heat Transfer, Part A, Applications*, Vol. 20, No. 1, 1991, pp. 95–110. doi:10.1080/10407789108944811

[9] Beck, J. V., and Osman, A. M., "Sequential Estimation of Temperature-Dependent Thermal Properties," *High Temperatures—High Pressures*, Vol. 23, No. 3, 1991, pp. 255–266.

[10] Dowding, K. J., Beck, J. V., Ulbrich, A., Blackwell, B. F., and Hayes, J., "Estimation of Thermal Properties and Surface Heat Flux in Carbon-Carbon Composite," *Journal of Thermophysics and Heat Transfer*, Vol. 9, No. 2, 1995, pp. 345–351. doi:10.2514/3.666

[11] Huang, C. H., and Yan, J. Y., "An Inverse Problem in Simultaneously Measuring Temperature-Dependent Thermal Conductivity and Heat Capacity," *International Journal of Heat and Mass Transfer*, Vol. 38, No. 18, 1995, pp. 3433–3441. doi:10.1016/0017-9310(95)00059-I

[12] Sawaf, B., Özisik, M. N., and Jarny, Y., "An Inverse Analysis to Estimate Linearly Temperature Dependent Thermal Conductivity Components and Heat Capacity of an Orthotropic Medium," *International Journal of Heat and Mass Transfer*, Vol. 38, No. 16, 1995, pp. 3005–3010. doi:10.1016/0017-9310(95)00044-A

[13] Dantas, L. B., and Orlande, H. R. B., "A Function Estimation Approach for Determining Temperature-Dependent Thermophysical Properties," *Inverse Problems in Engineering*, Vol. 3, No. 4, 1996, pp. 261–279. doi:10.1080/174159796088027627

[14] Dowding, K. J., Beck, J. V., and Blackwell, B. F., "Estimating Temperature-Dependent Thermal Properties," *Journal of Thermophysics and Heat Transfer*, Vol. 13, No. 3, 1999, pp. 328–336. doi:10.2514/2.6463

[15] Garcia, S., "Experimental Design Optimization and Thermophysical Parameter Estimation of Composite Materials Using Genetic Algorithms," Ph.D. Dissertation, Dept. of Mechanical Engineering, Virginia Polytechnic Inst. and State Univ., Blacksburg, VA, 1999.

[16] Alhama, F., Zueco, J., and González-Fernández, C. F., "An Efficient Method to Determine Thermal Conductivity and Specific Heat in Solids as an Inverse Problem," *International Communications in Heat and Mass Transfer*, Vol. 31, No. 7, 2004, pp. 929–937. doi:10.1016/j.icheatmasstransfer.2004.05.003

[17] Hakkaki-Fard, A., and Kowsary, F., "Heat Flux Estimation in a Charring Ablator," *Numerical Heat Transfer, Part A, Applications*, Vol. 53, No. 5, 2008, pp. 543–560. doi:10.1080/10407780701678240

[18] Loh, M. H., and Beck, J. V., "Simultaneous Estimation of Two Thermal Conductivity Components from Transient Two-Dimensional Experiments," American Society of Mechanical Engineers Paper 91-WA/HT-11, New York, 1991.

[19] Copenhaver, D. C., Scott, E. P., and Hanuska, A., "Thermal Characterization of Honeycomb Sandwich Structures," *Journal of Spacecraft and Rockets*, Vol. 35, No. 4, 1998, pp. 539–545. doi:10.2514/2.3364

[20] Aerotherm Chemical Equilibrium, Software Package, Ver. 81, Acurex Corp., Aerotherm Div., Mountain View, CA, Aug. 1981.

[21] Milos, F. S., and Chen, Y.-K., "Comprehensive Model for Multi-Component Ablation Thermochemistry," AIAA Paper 97-0141, Jan. 1997.

[22] Özisik, M. N., and Orlande, H. R. B., *Inverse Heat Transfer: Fundamentals and Applications*, Taylor and Francis, New York, 2000.

[23] Oliveira, A. P. D., and Orlande, H. R. B., "Estimation of the Heat Flux at the Surface of Ablating Materials by Using Temperature and Surface Position Measurements," *Inverse Problems in Science and Engineering*, Vol. 12, No. 5, 2004, pp. 563–577.

[24] Colaco, M. J., and Orlande, H. R. B., "Comparison of Different Versions of the Conjugate Gradient Method of Function Estimation," *Numerical Heat Transfer, Part A, Applications*, Vol. 36, No. 2, 1999, pp. 229–249. doi:10.1080/104077899274859

[25] Roache, P. J., *Verification and Validation in Computational Science and Engineering*, Hermosa Publishers, Albuquerque, NM, 1998, pp. 114–136.

[26] Hanak, J. P., "Experimental Verification of Optimal Experimental Designs for the Estimation of Thermal Properties of Composite Materials," M.S. Thesis, Dept. of Mechanical Engineering, Virginia Polytechnic Inst. and State Univ., Blacksburg, VA, 1995.

[27] Beck, J. V., "Determination of Optimum, Transient Experiments for Thermal Contact Conductance," *International Journal of Heat and Mass Transfer*, Vol. 12, No. 5, 1969, pp. 621–633. doi:10.1016/0017-9310(69)90043-X

[28] Taktak, R., Beck, J. V., and Scott, E. P., "Optimal Experimental Design for Estimating Thermal Properties of Composite Materials," *International Journal of Heat and Mass Transfer*, Vol. 36, No. 12, 1993, pp. 2977–2986. doi:10.1016/0017-9310(93)90027-4

[29] Moncman, D. A., "Optimal Experimental Designs for the Estimation of Thermal Properties of Composite Materials," M.S. Thesis, Dept. of Mechanical Engineering, Virginia Polytechnic Inst. and State Univ., Blacksburg, VA, 1994.

[30] Moncman, D. A., Hanak, J. P., Copenhaver, D. C., and Scott, E. P., "Optimal Experimental Designs for Estimating Thermal Properties," *Proceedings of the 4th ASME—JSME Thermal Engineering Joint Conference*, Vol. 3, American Society of Mechanical Engineers, New York, 1995, pp. 461–468.